Electronic Supplementary Material (ESI) for ChemComm.

Dual-Mode Nanoprobe for Evaluation of Autophagy Level Affected by Photothermal Therapy

Jia Liu, Yining Qu, Tingting Zheng* and Yang Tian*

Shanghai Key Laboratory of Green Chemistry and Chemical Processes, Department of Chemistry, School of Chemistry and Molecular Engineering, East China Normal University, Dongchuan Road 500, Shanghai 200241, P.R. China. Email: ttzheng@chem.ecnu.edu.cn; ytian@chem.ecnu.edu.cn

Contents:

S1. Experimental Sections

Chemicals and materials. Molybdenum powder (99.5%), H_2O_2 (30 wt %) and poly (ethylene oxide) with a molar mass of 10 K Da (PEG) were purchased from Aladdin. 3-(4, 5-dimethylthiazol-2yl)-2, 5-diphenyltetrazolium bromide (MTT) was obtained from Nanjing Keygen Biotech. Co., Ltd (Nanjing, China). The aptamer sequences were synthesized and purified by Shanghai Sangon Biological Engineering Technology & Services Co. (Shanghai, China). The microRNA sequences were synthesized and purified by Takara Biotechnology Co. Ltd. (Dalian, China). The sequences of the aptamers and microRNAs are listed in Table S1. All other reagents were of analytical grade. Ultrapure water (18.2 MΩ cm^{-1}) produced with a Milli-Q gradient system (Millipore, Billerica, MA) was used in all experiments.

Preparation of MoO_2-doping MoO_3 Nanospheres (MNPS). 60 mL of H_2O_2 (30 wt %) aqueous solution was slowly added into a beaker containing 4.78 g of Mo powder (50 mmol) with magnetic stirring in an ice−water bath. Then a yellow solution was formed and continuously stirred to drive off excess H_2O_2. Subsequently, the solution was diluted to 100 mL to make the Mo concentration of 0.5 mol/L. Then, 15 g of PEG was added to 20 mL of the above molybdenum precursor solution. Then the solution was magnetically stirred, forming a transparent yellow solution. Subsequently, the resulting solution was transferred to a poly(tetrafluoroethylene) (Teflon)-lined stainless steel autoclave (50 mL), which was sealed and treated at 80 °C for 12 h. A blue precipitate was collected by centrifugation and washed with water several times.

Characterizations of MoO_2-doping MoO_3 Nanospheres (MNPS). The morphologies and structures of MPNS were characterized by scanning electron micrographs (SEM), transmission electron micrographs (TEM), X-ray diffraction (XRD) and X-ray photoelectron spectroscopy (XPS). The TEM images were obtained using a S-4800 scanning electron microscope operated at an accelerating voltage of 200 kV. High resolution transmission electron micrographs (HRTEM) images were taking using a JEM-2100 transmission electron microscope with an accelerating voltage of 200kV. SEM measurements were performed using a field emission gun S-4800 scanning electron microscope (Hitachi, Japan). Raman enhanced scanning were performed on a Thermo Scientific DXR Raman Microscope with a 10X (NA 0.4) microscope and a 10mW laser power for SERS measurements.

Apt Loading. The aptamers (Apt 1 and Apt 2) and the (MNPS) solution mixed and stirred for 30 min. Then the mixture was washed 3 times, followed by centrifugation (12000 rpm, 10 min) to remove the excess unbinding aptamers. Finally, the aptamers-loaded MNPS, denoted as Apt@MNPS. To study the drug loading efficiency, we used the fluorescence spectrophotometer to quantify the loaded drugs.

Response of Apt@MNPS to miR-18a* and miR-4802. For Raman detection of the two kinds of miRNAs in vitro, the Apt@MNPS were immersed in PBS buffer containing various concentrations of miRNAs from 1 fM~100 nM. The Raman signal intensities of Cy5 and ROX in the withdrawn solution were measured by 785 nm laser through the Raman scanning. For fluorescence detection, the Apt@MNPS were immersed in PBS buffer containing various concentrations of miRNAs from 10 fM~300 nM. The fluorescence intensities of Cy5 and ROX were monitored by 552 nm laser.

Cell Culture. MCF-7 cells were obtained from Sciencell Inc and cultured in Dulbeccoccoo Dufied Eagle Medium (DMEM) at 37 °C under 5% CO_2 atmosphere, supplemented with L-glutamine (2 mM), penicillin (100 units mL^{-1}), streptomycin (100 μg mL^{-1}), and 10% fetal bovine serum (FBS). At the logarithmic growth phase, the cells were collected and separated from the medium by centrifugation at 800 rpm for 3 min and then resuspended in the buffer to obtain a homogeneous cell suspension. The cell number was determined using a Petroff-Hausser cell counter (USA). The cell pellets were suspended in 1 mL of lysis solution. Serum-free medium (Opti-MEM) was used during the transfection process.

Cytotoxicity Assay. MCF-7 cells were seeded in a 96-well cell culture plate 24 h prior to material treatments at a density of 1×10^4 cells/well. After 24 h, the cells were treated with different concentrations of MNPS at 37°C, 5% CO_2 for 12 h, respectively. And the control cells were treated with equivalent volume of PBS. For PTT, the MNPS or MNPS+CQ treated cells were exposed to 808 nm near-infrared laser (1 W/cm^2) for 10 min. After light irradiation treatments, the supernatant was removed and replaced by fresh cell culture medium. Then, the cells were further cultured for 12h. Cytotoxicity was determined by performing the MTT assay. 20 μL of MTT solution (5 mg/mL) was added into each well, followed by incubating for another 4 h to allow the formation of formazan dye. Then, 80 μL of DMSO was added to terminate the reaction after removing the medium. Absorbance at 490 nm was measured

through a Varioskan LUX-multimode microplate reader (Thermo Fisher Scientific, USA) and the cell viability was determined by calculating the absorbance result. Cell viability (%) = the absorbance of experimental group/the absorbance of blank control group × 100%.

Western Blot. The MCF-7 cells were collected and resuspended with 100 μL lysis buffer [50 mM Tris-HCl (pH 8.0), 150 mM NaCl, 1% (v/v) Triton-X 100, and protease inhibitor]. After the samples were estimated by BCA kit (Applygen), the samples (~60 μg) were subjected to SDS-PAGE and then transferred to a nitrocellulose membrane blot. Next, nitrocellulose membrane blots were blocked with a blocking buffer [5% (wt/v) nonfat milk, 0.1% (v/v) Tween 20 in 0.01 M TBS], then incubated with primary antibodies overnight at 4 °C, and incubated with a secondary antibody for 2 h at room temperature. Finally, Typhoon Trio Variable Mode Imager was used to obtain the images. Band density was calculated by NIH ImageJ software.

S2. Additional Figures

1. Sequence of aptamers and miRNAs (Table S1)

The nucleotides signed in blue were the mismatched parts. The NT was non-target sequence. Let-7b was selected as a NT sequence because it was considered as a typical biomarker of breast cancer, but its sequence differed markedly from that of target miRNAs.

Name	Sequence(5'-3')
Aptamer1 (Apt1)	CCAGAAGGAGCACTTAGGGCAGT-Cy5
Aptamer2 (Apt2)	AACATGGTCTAGAACCTCCATA-ROX
miR-18a* mimics	ACUGCCCUAAGUGCUCCUUCUGG
1-MT for miR-18a*	ACUGCCCUCAGUGCUCCUUCUGG
3-MT for miR-18a*	AGUGCCCUCAGUGCUCCUACUGG
miR-4802 mimics	UAUGGAGGUUCUAGACCAUGUU
1-MT for miR-4802	UAUGGAGGCUCUAGACCAUGUU
3-MT for miR-4802	UGUGGAGGCUCUAGACCACGUU
NT	UGAGGUAGUAGGUUGUGUGGUU
miR-21	UAGCUUAUCAGACUGAUGUUGA
miR-155	UUAAUGCUAAUCGUGAUAGGGU
miR-210	CUGUGCGUGUGACAGCGGCUGA
miR-375	UUUGUUCGUUCGGCUCGCGUGA
miR-373	ACUCAAAAUGGGGGCGCUUUCC

Table S1. Sequence of aptamers and miRNAs.

2. Characterization of MNPS (Figure S1)

The FT-IR spectrum of MNPS (Fig. S1d) demonstrates that the absorption peaks in the region of 500-800 cm^{-1} are the characteristics of the Mo-O-Mo stretching vibrations, and the peak at 1002 cm^{-1} and one peak at 3408 cm^{-1} are attributed to the Mo=O and O-H stretching vibrations. In addition, the bending vibrations of C-H located at 2830 and 2986 cm^{-1}, and C-O at 1153 cm^{-1} originate from PEG.

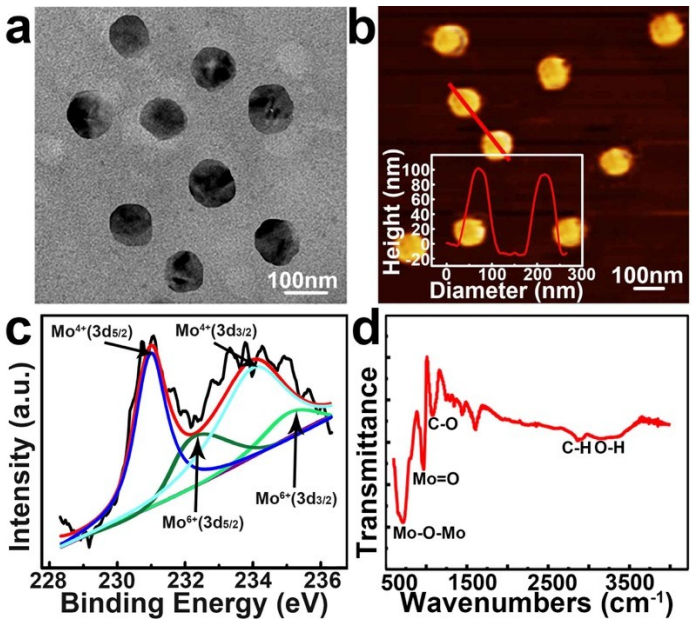

Figure S1. (a) Transmission electron microscopic (TEM) and (b) Atomic force microscopy (AFM) images of MNPS. (c) X-ray photoelectron and (d) Fourier-transform infrared (FT-IR) spectra of MNPS.

3. Calculation of enhancement factor (EF) (Figure S2)

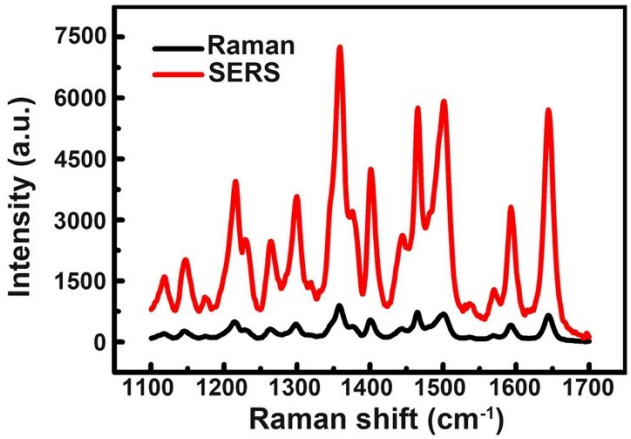

Figure S2. Raman and SERS spectra of Apt absorbed on the silica slide and slide covered with MNPS.

The enhancement factor (EF) of MNPS was calculated by the following equation：

$EF=I_{SERS}N_{Raman}/I_{Raman}N_{SERS}$

Where I_{SERS} and I_{Raman} are the intensities of selected Raman peak in the SERS and normal Raman spectra. N_{SERS} and N_{Raman} are the average number of molecules in scattering for SERS and normal Raman measurement.

The peak at 1644 cm^{-1} was taken as the characteristics of ROX for example, the intensity of $I_{SERS}$and I_{Raman} were 5806 and 654. Then, N_{Raman}=1 M x 20 μL, N_{SERS}=5 μM x 20 μL. Thus, the EF value for ROX on MNPS was calculated to be 1.78 x 10^6.

In addition, the peak at 1592 cm^{-1} was taken as the characteristics of Cy5 for example, the intensity of I_{SERS} and I_{Raman} were 3388 and 354. Then, N_{Raman}=1 M x 20 μL, N_{SERS}=5 μM x 20 μL. Thus, the EF for Cy5 on MNPS was calculated to be 1.91 x 10^6.

4. Mechanism of chemical enhancement (Figure S3)

The EF value for Cy5 on MNPS was higher than ROX, which was attributed to the charge transfer (CT) induced chemical enhancement. To elucidate the CT process between MNPS and Cy5/ROX molecules, we determined the conductive band (CB) and valence band (VB) of MNPS, and the highest occupied molecular orbital (HOMO) and the lowest unoccupied molecular orbital (LUMO) levels of Cy5 and ROX molecules. The VB levels of MoO_2 and MoO_3 were -4.02 eV and -4.56 eV, and the CB levels of MoO_2 and MoO_3 were -1.62 eV and -0.25 eV, respectively. While the HOMO and LUMO levels of report molecules were -5.85 and -3.46 eV for Cy5, and -7.13 and -2.21 eV for ROX, respectively. In the Cy5-MoO_3 system, the energy barrier from the VB of MoO_3 to LUMO of Cy5 was 1.20 eV. With the introduction of MoO_2 to the MoO_3 system, charge redistribution occurred, which led to the alignment of the energy levels between MoO_2 and MoO_3. In this case, the narrow energy barrier was 0.64 eV from VB of MoO_3 to VB of MoO_2 and 0.56 eV from VB of MoO_2 to LUMO of Cy5, respectively, which were smaller than that in pure MoO_3 system. Whereas, CT cannot be observed between ROX and substrates, because the 785 laser cannot provide sufficient energy for the electron transition from VB of MoO_2 to LUMO of ROX. The results illustrated the EF value for Cy5 on MNPS was higher than that for ROX on MNPS.

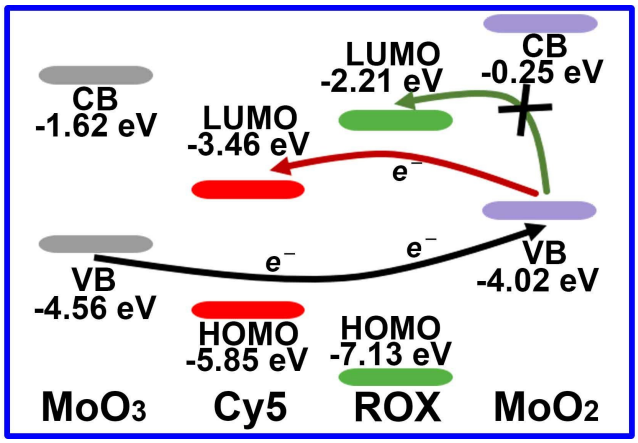

Figure S3. Mechanism of chemical enhancement fo Cy5 and ROX on MNPS.

5. Principle of FRET of Apt on MNPS (Figure S4)

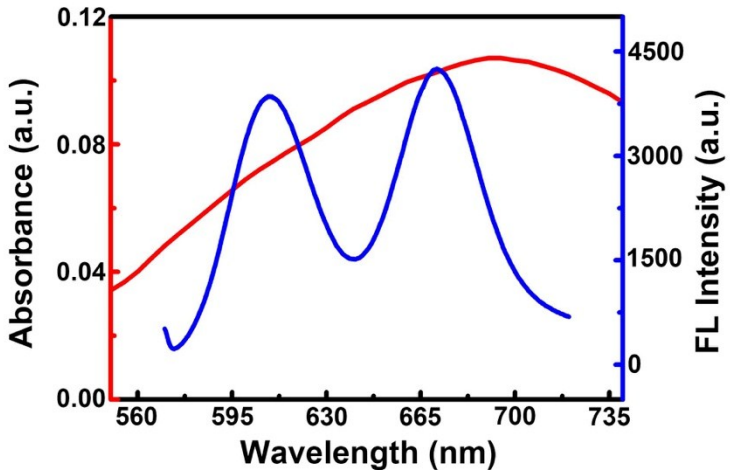

Figure S4. Principle of fluorescence quenching of Apt on MNPS. The fluorescence emissions of Apt (λex=552 nm) were covered by the absorbance of MNPS from 560-735 nm, which indicated the occurrence of fluorescence resonance energy transfer (FRET) between Apt and MNPS.

6. Space interaction between signal molecule and MNPS (Figure S5)

The FAM molecule, which fluorescence emission could not match the absorption of MNPS, was chosen for this determination. The FAM molecules were mixed with MNPS, then the fluorescence change of FAM was detected and observed in Figure S5. The fluorescence intensity of FAM exhibited a slight decline after mixing with MNPS, indicating the weak contribution of space interaction. Therefore, there existed double energy transfer processes in our system.

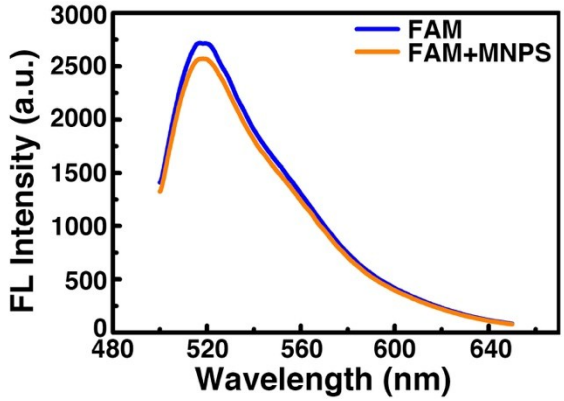

Figure S5. Fluorescence spectra of FAM before (blue line) and after mixing with MNPS (orange line).

7. Feasibility of detection for miR-18a* and miR-4802 (Figure S6)

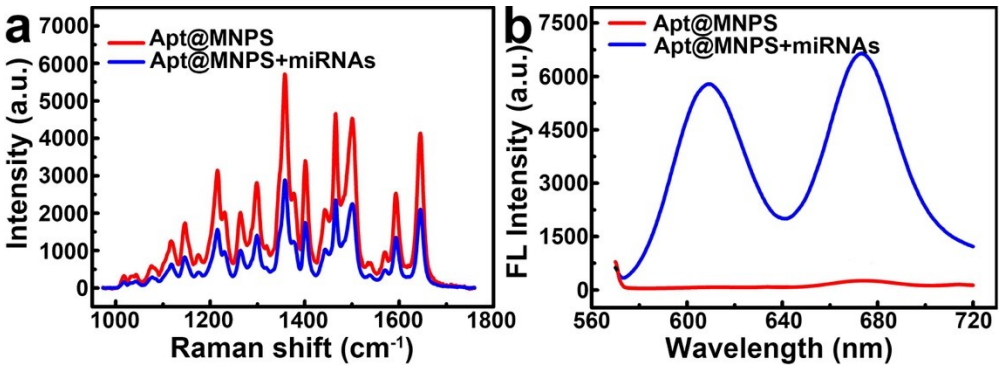

Figure S6. SERS (a) and Fluorescence (b) spectra of Cy5-tagged Apt1 and ROX-tagged Apt2 on MNPS without (red line) and with (blue line) the addition of miR-18a* and miR-4802.

8. Aptamers loading capacity on MNPS (Figure S7)

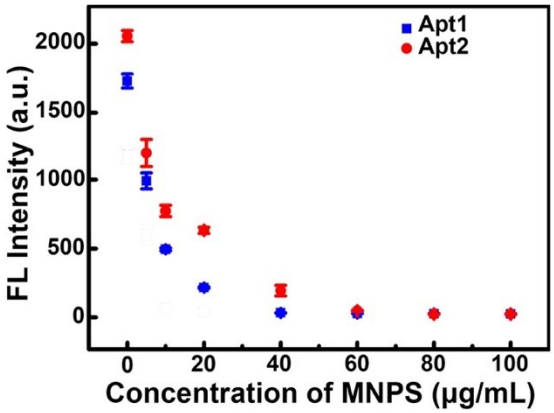

Figure S7. The fluorescence dot plot for aptamers loading capacity. The concentration of Cy5-tagged Apt1 and ROX-tagged Apt2 were 20 μM. The optimal concentration of MNPS was 60 μg/mL.

9. Selectivity of Apt@MNPS (Figure S8 and S9)

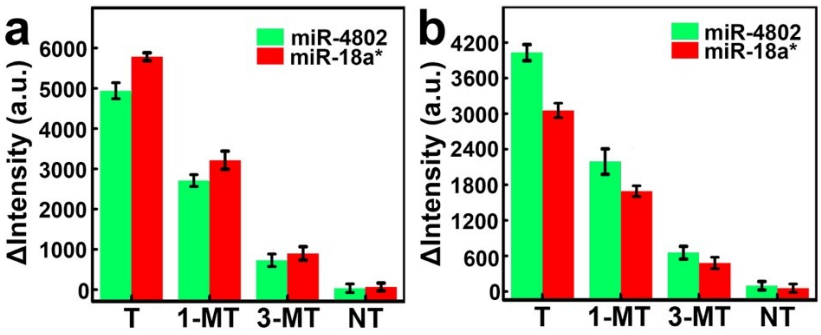

Figure S8. (a) Fluorescence bars for evolution of the selectivity. (b) SERS bars for evolution of the selectivity. T: target miRNAs, 1-MT: single-base mismatched target, 3-MT: three-base mismatched target, NT: non-target.

Several kinds of miRNAs overexpressed in the breast cancer cells were employed for further confirming the selectivity of this nanoprobe. As depicted in Figure S9a and S9b, both of fluorescence and Raman intensities change towards target miRNAs were significantly higher than the miRNAs overexpressed in the breast cancer cells, indicating the good selectivity of this nanoprobe we developed.

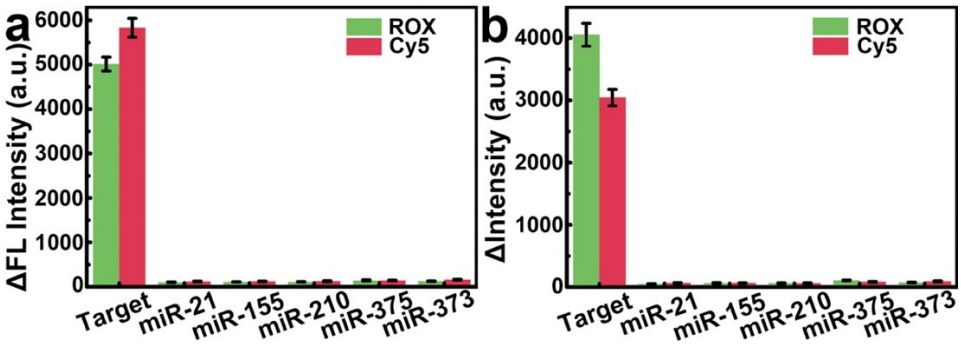

Figure S9. Fluorescence (a) and SERS (b) bars for evolution of the selectivity of Apt@MNPS.

10. Cross-Talk between miR-18a* and miR-4802 (Figure S10)

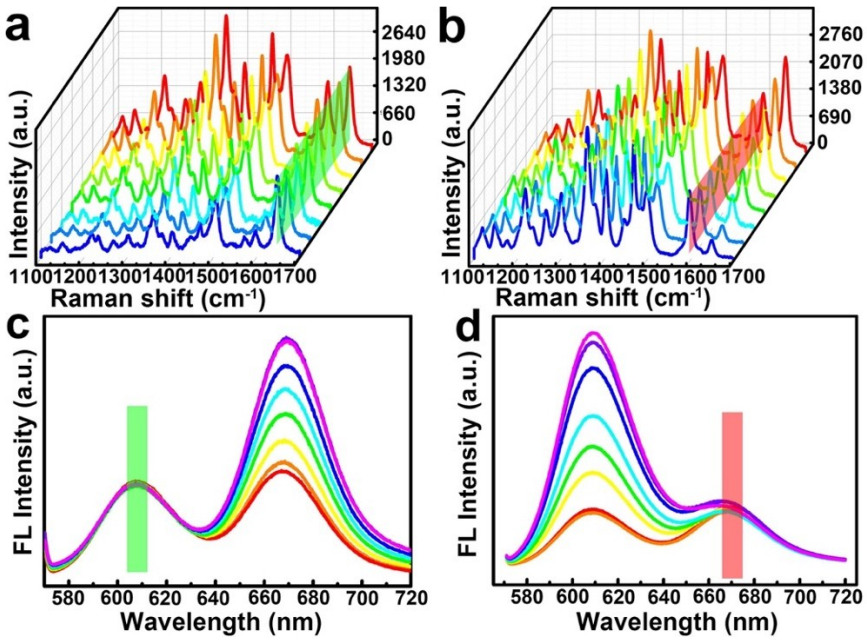

Figure S10. Evaluation of cross reaction for monitoring miR-4802 (green shadow) and miR-18a* (red shadow) by SERS (a-b) and fluorescence (c-d) methods.

11. Photothermal property of MNPS (Figure S11)

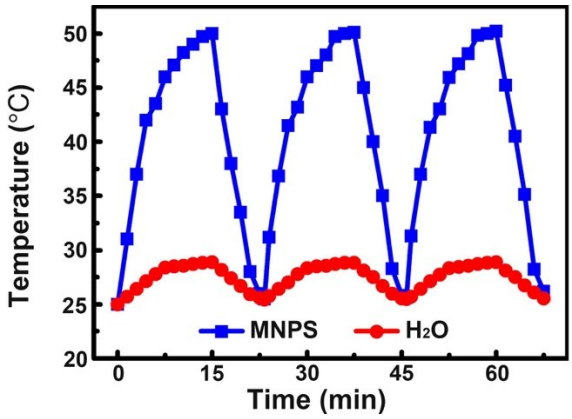

Figure S11. Temperature evolutions of MNPS and of pure water upon exposure to 808 nm laser irradiation at 1 W cm^{-2}.

12. Signal stability under different temperatures (Figure S12 and S13)

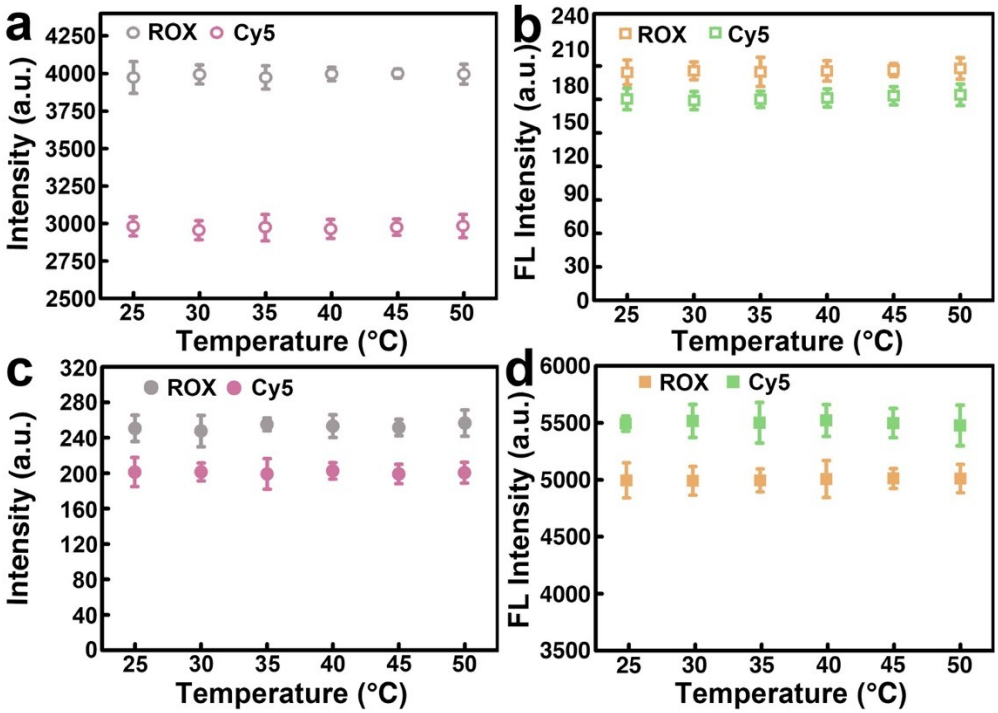

Figure S12. SERS (a) and fluorescence (b) signal stability of Apt@MNPS upon exposure to different temperatures. SERS (c) and fluorescence (d) signal intensities of Apt@MNPS under different temperatures with the addition of 100 nM miRNAs.

To ensure the stability between aptamers and nanospheres in the medium when the temperature was increased, the aptamers modified nanospheres were incubated in the PBS buffer and cell culture medium under the temperature from 25 to 50 degrees, respectively. After 4 h, the solutions were centrifuged, and the supernatants were detected by fluorescence spectrometer. As shown in Figure S13a, fluorescence intensities in the PBS buffer showed very weak signals when the temperature increased from 25 to 50 degrees. Meanwhile, no significant fluorescence intensities of I_{610} and I_{670} in the cell culture medium were observed in Figure S13b. Thus, the results demonstrated that the aptamers kept attached on the surface of nanospheres in PBS and cell culture mediums even when the temperature increased to 50 degrees.

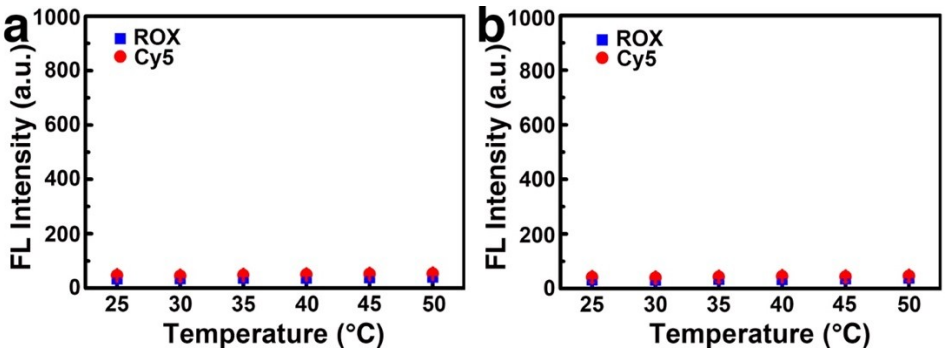

Figure S13. Fluorescence intenisties of Cy5 and ROX in the supernatants of PBS buffer (a) and cell medium (b).

13. Cytotoxicity of MNPS against MCF-7 cells (Figure S14 and S15)

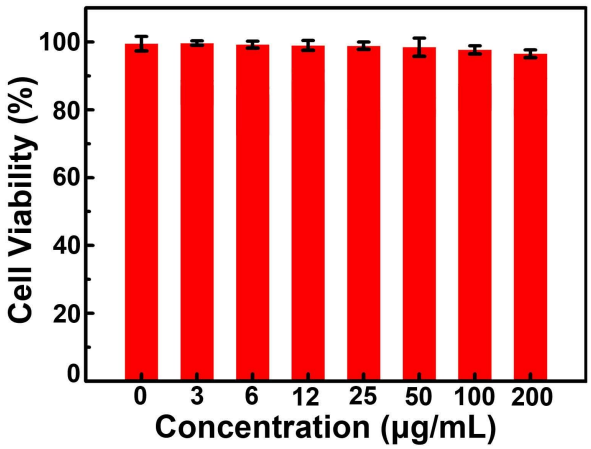

Figure S14. In vitro cytotoxicity of different concentration of MNPS against MCF-7.

ROS production/lipid peroxidation assays were further performed for verifying the results. First of all, cells were incubated with 10 μmol/L of the fluorescent probe 2'-7'-dichlorodihydrofluorescein diacetate (CM-H2DCFDA) for 30 min at 37 ℃ and the level of fluorescence was determined. Meanwhile, the OxiSelect TBARS assay kit was used to determine the level of lipid peroxidation by measuring malondialdehyde (MDA). As shown in Figure S15a and S15b, ROS production/lipid peroxidation data indicated that nanoparticles had no additional interference to therapy under the photothermal effects. Then, flow cytometry analysis was used for further verifying the accuracy of MTT results. As shown in Figure S15c, all the rates of live cells were higher than 95% after the cells were incubated with different concentrations (0-200 μg/mL) of our nanoprobes, which was consistent with the results of MTT assay.

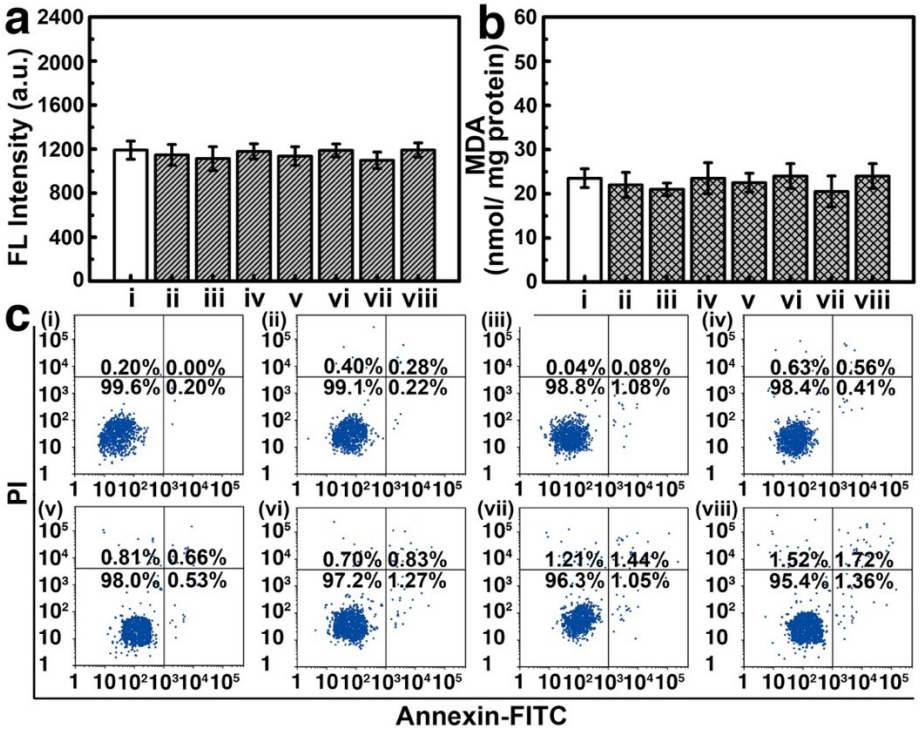

Figure S15. (a) Fluorescence intensity of DCFDA in cells treated with different concentrations of nanoparticles. (b) MDA level in cells treated with different concentrations of nanoparticles. (c) Flow cytometry analysis of cell apoptosis induced by different concentrations of nanoparticles, i-viii were corresponding to 0, 3, 6, 12, 25, 50, 100 and 200 μg/mL nanoparticles.

14. Intracellular location of Apt@MNPS (Figure S16)

The probe was located in the cell, which was proved as follows. Three-dimensional images of entire cells stained by Apt@MNPS were obtained. MCF-7 cells stained by Apt@MNPS were imaged at different depths along the Z-axis. Micrographs were taken while the focal plane was moved in incremental depths from the bottom of cells up to the coverslip. A typical section image (Figure S16) demonstrated that the probes we developed were present in the cell instead of adsorbing on the surface of cell.

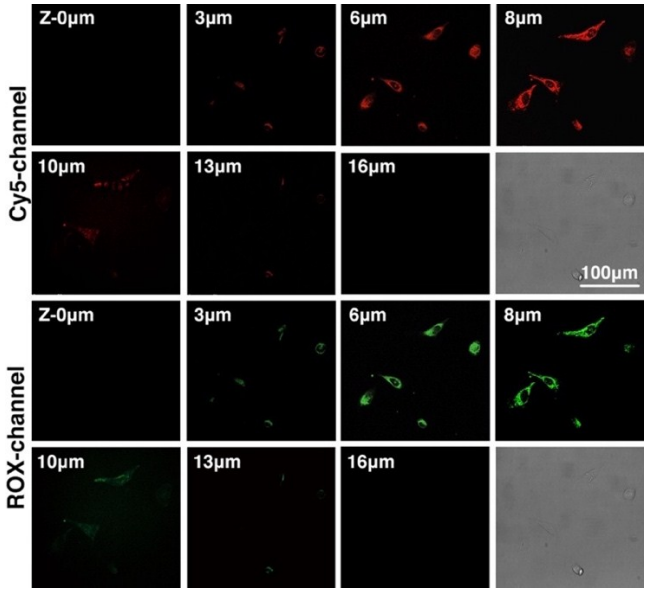

Figure S16. Z-Axis scanning image of internalized Apt@MNPS recorded by confocal microscope. Micrographs were taken while the focal plane was moved in incremental steps from the bottom of the cell up to the coverslip.

15. Intracellular responsive time (Figure S17 and Figure S18)

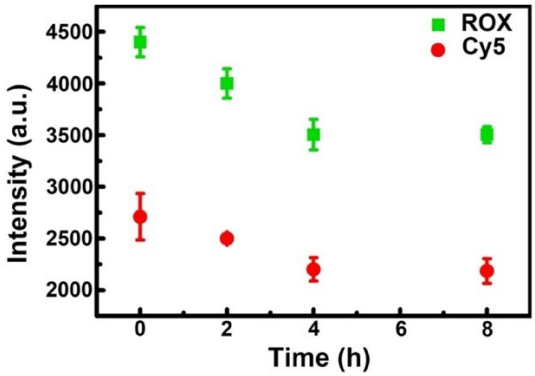

Figure S17. SERS evolution of Cy5 and ROX in MCF-7 cells incubated with MNPS for 0 h, 2 h, 4 h and 8 h, respectively.

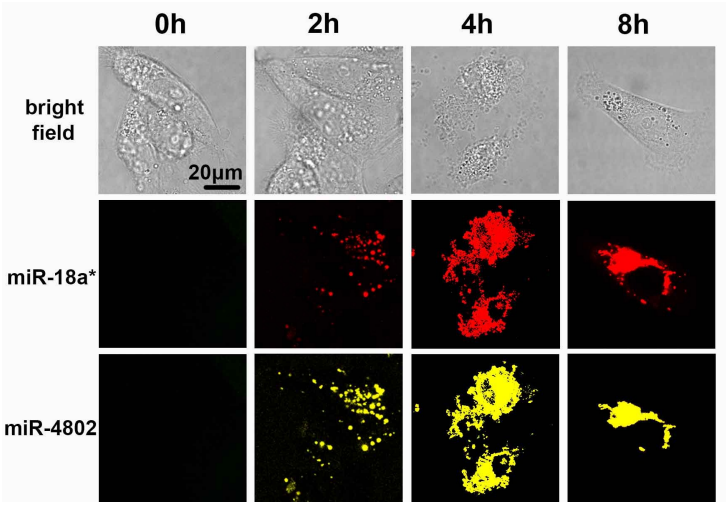

Figure S18. Fluorescence images of miR-18a* and miR-4802 in MCF-7 cells incubated with MNPS for 0 h, 2 h, 4 h and 8 h, respectively.

16. Western blot analysis of autophagy (Figure S19)

Western blot, a standard method, was utilized for demonstrating the effect of PTT on autophagy. As shown in Fig. S19a and S19b, the LC3 II/β-actin ratio increased with the function of PTT and restored to the original level after the addition of CQ, indicating also demonstrated that the autophagy was indeed activated by PTT.

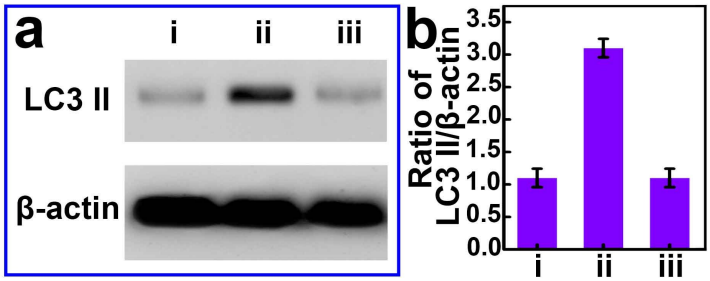

Figure S19. (a) Western blot analysis of autophagy induced by control (i), MNPS+Light (ii), MNPS+Light+CQ (iii). (b) Quantitative analysis of Western blot results from (a).

17. Cytotoxicity of MNPS-induced PTT (Figure S20)

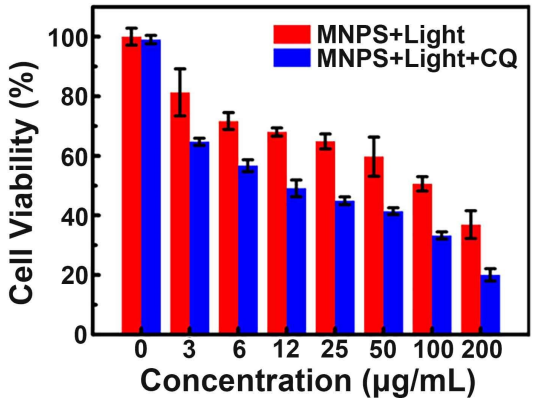

Figure S20. In vitro cytotoxicity of MNPS-induced PTT and the synergy of PTT and CQ.